Journal of Manufacturing Processes 86 (2023) 98–108

Contents lists available at ScienceDirect

Journal of Manufacturing Processes

journal homepage: www.elsevier.com/locate/manpro

A cold spray-based novel manufacturing route for flexible electronics

Semih Akin [a], Seunghwan Jo [a], Martin Byung-Guk Jun [a,b,*]

[a] School of Mechanical Engineering, Purdue University, West Lafayette, IN 47907, USA
[b] Indiana Manufacturing Competitiveness Center (IN-MaC), Purdue University, West Lafayette, IN 47907, USA

ARTICLE INFO

Keywords:
Flexible electronics
Additive manufacturing
Cold spray
Femtosecond laser machining
Ultrasonic welding
Microheater

ABSTRACT

In this research, we propose a cold spray-based novel manufacturing route that enables the custom production of flexible electronics (FE) at high spatial resolution without a need of high-temperature post-sintering process. The proposed manufacturing route sequentially comprises: (1) cold spray metallization; (2) femtosecond laser machining; and (3) ultrasonic plastic welding. First, the flexible polymer (*i.e.*, PET) surface is metallized by cold spray direct writing of Tin (Sn) particles under vacuum-and mask-free conditions. The as-metallized polymer film is then precisely cut into arbitrarily designed high-resolution electrodes (*i.e.*, 500 μm linewidth) by femtosecond laser machining. Lastly, the laser-cut electrodes are joined onto a base polymer substrate *via* ultrasonic plastic welding to constitute mechanically resilient and conformal FE. In this way, the proposed route enables exploiting the unique features of cold spray deposits in FE (*e.g.*, strong adhesion, high conductivity, minimal thermal input). The resultant printings show excellent electrical conductivity (1.08×10^6 S·m^{-1}), flexibility (60 % elongation), and adhesion strength without significantly compromising intrinsic polymer and functional coating properties. Moreover, a serpentine-shaped flexible microheater (10×10 mm^2) is also fabricated to demonstrate the viability of the introduced platform in flexible microelectronics. This work potentially provides a promising route toward the rapid, scalable, and cost-effective production of high-resolution and high-performance FE in a mechanically resilient and conformal manner.

1. Introduction

Flexible electronics (FE) is of particular interest in smart films [1], wearable sensors [2–4], robotic [5], energy harvesting [6], food packaging [7], and optoelectronics [8] owing to its unique characteristics, including recyclability, durability, low-carbon footprint, cost-effectiveness, and compatibility with soft materials and curvilinear surfaces [9–11]. These important features of FE enable high-fidelity performance over conventional wafer and circuit board technologies. FE is generally produced through additive patterning of functional coating materials (*i.e.*, typically nanomaterial inks) on a flexible target surface in various designs. Traditional patterning approaches to produce FE mainly involve inkjet printing [12,13], screen printing [14], gravure printing [15], blade printing [16], aerosol jet printing [17,18], or hybrid printing methods [19]. In these approaches, functional coating materials (*i.e.*, typically nanomaterial inks) are transferred onto the target surface either by physical contact (*e.g.*, screen printing, gravure printing, offset printing, *etc.*) or non-contact (*e.g.*, inkjet printing, aerosol jet printing) [20,21].

As for physical contact printing, paste-like coating materials (ink) are transferred onto the target surface by either hand or using semi or fully-automated rolling systems [22]. Physical contact printing methods, however, often need a shadow mask for precise patterning of the circuits at desired size and shape, thereby increasing the process costs. In case of non-contact printing methods, nanomaterials in the form of colloidal dispersion are deposited by the means of a printing nozzle under controlled settings without direct contact, which in turn reduces nozzle and substrate contamination. The advantages of non-contact printing methods include rapid and accurate deposition of a broad range of functional materials over a large area in a maskless fashion [11]. Hybrid printing method involves the integration of various printing techniques to fabricate FE [23]. Typically, hybrid printing is conducted by coupling direct ink writing of conductive and dielectric materials (*i.e.*, multi-material based) within an integrated additive manufacturing platform [19]. Through hybrid printing, multilayered flexible circuits can be created by printing conductive and insulator materials alternatively for each layer [23].

In the production of FE, precise control of the patterning at high spatial resolution is vital to ensure the mechanical and electrical

* Corresponding author at: School of Mechanical Engineering, Purdue University, West Lafayette, IN 47907, USA.
E-mail address: mbgjun@purdue.edu (M.B.-G. Jun).

https://doi.org/10.1016/j.jmapro.2022.12.035
Received 10 November 2022; Received in revised form 15 December 2022; Accepted 16 December 2022
Available online 3 January 2023

Nomenclature

Symbol

A	Area
L	Length
P	Power
R	Resistance
R/R_0	Relative resistance
R_s	Sheet resistance
t	Thickness
w	width
ρ	Resistivity
Ω	Ohm

Abbreviations

CS	Cold spray
FE	Flexible electronics
OM	Optical microscopy
PET	Polyethylene terephthalate
PEN	Polyethylene naphthalate
PI	Polyimide
SEM	Scanning electron microscopy
Sn	Tin
UTS	Ultimate tensile strength
UW	Ultrasonic welding

reliability of the resultant printings to achieve high-performance electronic devices. Despite great advances, traditional manufacturing approaches have limitations in achieving ultra-fine patterning without the need for a dedicated mask and/or vacuum equipment. Moreover, conventional printing methods often suffer from low adhesion strength and poor conductivity, thereby requiring a high-temperature post-annealing (sintering) process to increase the adhesion strength and conductivity of the resultant printings [11]. Post-sintering processes, however, lead to fast oxidation of the functional coatings while increasing the manufacturing cost. Also, post-annealing limits the use of low-thermal budget flexible substrates such as polyethylene terephthalate (PET) and polyethylene naphthalate (PEN), which are highly demanded substrates in FE owing to their inherent advantages (*e.g.*, optical transparency, various thickness, low-cost, recyclability, *etc.*) [9,11,24]. As such, to confront the abovementioned challenges, a non-traditional manufacturing approach that enables high-throughput production of high-resolution FE at low processing temperatures with enhanced electrical conductivity and adhesion strength is of great necessity.

Most recently, the authors' group employed the cold spray (CS) particle deposition technique for rapid and scalable production of FE, and viable results have been achieved [25]. More specifically, owing to unique features of the CS technique (*e.g.*, low-process temperature, strong adhesion strength, scalability, high deposition rate [26,27]), millimeter-scale Tin (Sn) electrodes were directly fabricated on a flexible polymer surface (PET) at low-operating temperatures (*i.e.*, <80 °C) [25]. In the same study [25], to address the low-resolution of CS, a subsequent femtosecond laser machining process was also conducted to achieve micron-scale flexible electrodes. Despite these successes, the fabricated microelectrodes through this approach suffer from poor mechanical resilience and conformity due to the electrodes' ultra-thin features. In detail, these ultra-fine electrodes over-hang without the support of a base-substrate, thereby limiting its use in FE applications. As such, after laser cutting, transferring the microelectrodes on a base polymer substrate is a vital necessity to exploit the unique properties of the CS process (*i.e.*, high deposition rate, strong adhesion strength, no need for post-sintering) in producing compact, resilient, and conformal flexible microelectronics.

In the current study, to fill the aforementioned critical gap, we extend our previous work [25] by proposing a novel manufacturing route that enables to exploit the unique features of the CS technique in FE. The proposed manufacturing route sequentially involves 1) cold spray metallization, 2) femtosecond laser machining, and 3) ultrasonic plastic welding processes to produce custom-designed FE at ambient conditions in a mask-and vacuum-free fashion. The surface of the flexible polymer (PET) is conductively metallized by the direct CS writing of Sn particles. As-metallized PET samples are then precisely cut into arbitrarily-designed high-resolution electrodes by laser machining. Lastly, the cut-off electrodes are transferred onto the base polymer (PET) substrate *via* ultrasonic plastic welding. The ultrasonic welding process ensures conformal and intimate contact of the electrodes on the base polymer substrate with improved mechanical resilience. The resultant printings are comprehensively characterized in terms of microstructure, mechanical strength, electrical conductivity, and adhesion strength. Leveraging the process settings, a flexible microheater (10×10 mm^2) is also fabricated to demonstrate the viability and applicability of the proposed manufacturing platform in flexible microelectronics. Moreover, the feasibility of the proposed approach is evaluated for a thermoset substrate material such as Kapton (polyimide) film, which is another highly demanded material for wearable electronics and smart film applications. The key and innovative contribution of the present work is the development of a complete CS-based manufacturing approach for custom-design, high-resolution, resilient, and conformal FE without the need for a post-sintering process.

2. Experimental section

2.1. Materials

Tin (Sn) particles (Centerline-SST Inc.) were used as the cold spray (CS) feedstock material owing to its corrosion resistance, soft nature (*i.e.*, HV = 11 [28]), low melting point (232 °C), and sprayability on various substrates [29]. These features of the Sn particles facilitate the metallurgical bonding of the particles on the target surface, which allows for electrically conductive functional printing (coating) on various polymers (*e.g.*, ABS, PEEK, CFRP, PET, PTFE, *etc.* [28,30,31]). As for the substrate material, polyethylene terephthalate (PET) polymer sheet (0.25 mm in thickness, McMaster-Carr, USA) was employed as a flexible substrate due to its inherent advantages in printed electronics including low-cost, optical transparency, recyclability, *etc.* [24]. The surface of PET samples was cleaned before and after each process to prevent possible contamination.

2.2. Methodology

Fig. 1 illustrates the proposed manufacturing route that sequentially involves: (1) CS metallization of the polymer substrate; (2) femtosecond laser machining (cutting) of the as-cold sprayed samples into arbitrary-designed electrodes (*e.g.*, Purdue University logo); and (3) transferring the laser-cut electrodes onto the base substrate (PET) *via* ultrasonic plastic welding. Unlike traditional manufacturing methods, the described approach is mask-free, and all the process steps are conducted under ambient conditions. Below, the detailed experimental procedures for each process are elaborated. Note that in the present study, the term "as-cold spayed" refers to solely CS metallized polymer, while the "resultant printing" corresponds to the ultrasonically welded electrodes on the base polymer surface right after laser cutting (see Fig. 1).

2.2.1. Cold spray metallization

Cold spray (CS) is an emerging solid-state surface metallization technique on various substrates [32]. CS relies on the high-speed impact of particles (*i.e.*, typically micron-scale metal particles) onto a target surface at low temperatures. In the CS technique, as shown in Fig. 2a, the particles are accelerated to high velocities (*e.g.*, supersonic) through a

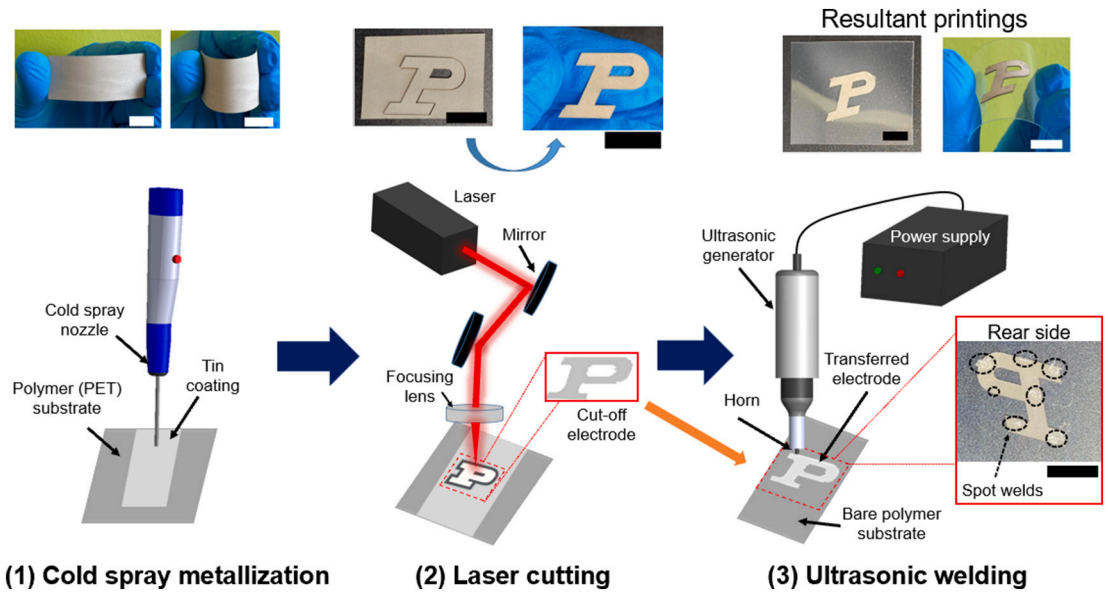

Fig. 1. The schematic of the proposed manufacturing route (scale bar 10 mm in all figures).

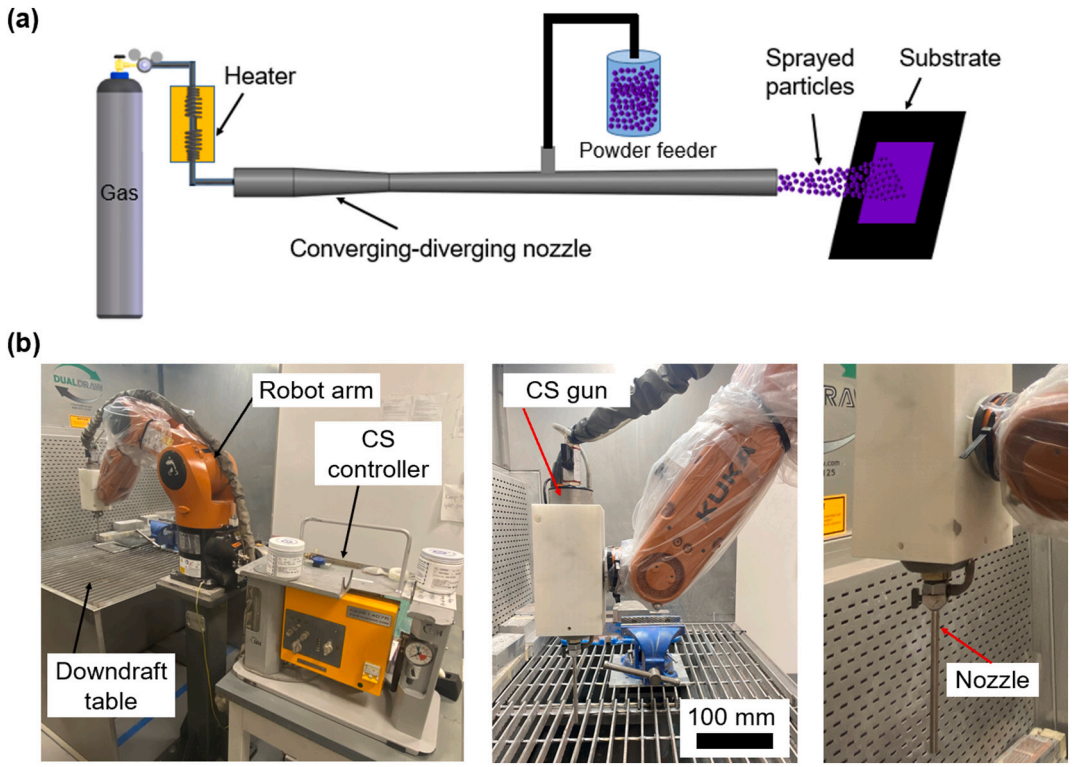

Fig. 2. (a) The schematic of a typical low-pressure cold spray process; (b) Representative images of the cold spray experimental setup.

converging-diverging nozzle, then impact a target surface. Under high-speed impingement, the particles' kinetic energy dissipates over the substrate surface, resulting in a high-strength functional coating/printing [27,32–34]. Given its high-throughput, scalability, and cost-effectiveness, the CS is a promising technique for rapid metallization on numerous surfaces [32,35].

In the present work, as shown in Fig. 2b, a low-pressure CS machine (Rus Sonic Inc., Model no: K205/407R) with the axisymmetric nozzle configuration was used in the particle deposition experiments. To precisely control the CS process, the nozzle gun was mounted on a programmable multi-axis robot arm (Kuka KR Agilus). Micron-scale (5–45 μm) Sn particles were cold sprayed on the PET surface to achieve millimeter-scale electrodes by direct writing of the Sn particles. The kinematic parameters of the CS process were adopted from the authors' previous work [25] that uncovered the process-structure-property relationships of CS direct writing of Sn particles on the PET substrate. The operational parameters of each procedure in the proposed manufacturing route are listed in Table 1.

2.2.2. *Femtosecond laser machining*

As-cold spray metallized polymer samples were cut out arbitrarily-designed micron-scale electrodes by the laser machining (cutting)

Table 1
Experimental parameters and their settings.

Procedure	Parameter	Setting	Unit
(1) Cold spray	Driving gas type	Air	–
	Driving gas pressure	0.7	MPa
	Driving gas temperature	80	°C
	Powder feed rate	0.2	$g{\cdot}s^{-1}$
	Nozzle transverse speed	75	$mm{\cdot}s^{-1}$
	Spray distance	10	mm
	Number of spray pass	1	–
(2) Laser machining	Wavelength	515	nm
	Pulse duration	229	fs
	Repetition rate	2	kHz
	Pulse energy	57	μJ
(3) Ultrasonic welding	Power	250–500	W
	Frequency	30	kHz
	Weld time	1	s

process. A femtosecond laser (04-1000, CARBIDE [36,37]) was employed to cut the as-cold sprayed polymer samples. Notably, the PET film is vulnerable to heat accumulation by the laser beam. Particularly, the laser pulse repetition larger than a threshold (*i.e.*, >10 kHz) led to undesirable heat accumulation on the metallized PET layer, resulting in localized deformation and cracks in the Sn coating (see Fig. S1, Supporting Information). Further increase in the laser repetition rate up to 60 kHz severely damaged the electrodes by propagating the heat-affected zone on the as-cold sprayed layer (Fig. S2, Supporting Information). Given these initial test results, we accordingly selected the laser parameters to cut out the as-cold sprayed PET film in a pre-programmed manner without delaminating the polymer substrate while minimizing the heat-affected zone. As such, the appropriate laser settings were occulted at the wavelength of 515 nm with a pulse duration of 229 fs, a repetition rate of 2 kHz, and a pulse energy of 57 μJ.

2.2.3. Ultrasonic plastic welding

Although laser machining can enable cutting high-resolution (*i.e.*, 30 μm linewidth) Sn electrodes through the PET substrate, it is vital to transfer the cut-off electrodes on a flexible base substrate to constitute compact and conformal FE devices. It is crucial to improve the mechanical and structural resilience of the electrodes for fabricating high-performance FE. In this regard, the laser-cut samples were transferred (joint) on a base (bare) PET polymer surface using the ultrasonic plastic welding technique to constitute high-resolution FE. Ultrasonic welding (UW) was employed owing to its intrinsic advantages of ultra-fastness, excellent bond strength, minimal surface damage, and low-cost [38,39]. An ultrasonic spot-welding setup that can provide a power of 500 W was used in the experiments. A representative image of the UW setup is shown in Fig. 3. In general, a UW system is a sequential assembly of four components (*i.e.*, generator, transducer, booster, and horn). The UW setup in Fig. 3 has an 8-mm diameter horn including a convex-shaped welding tip (*i.e.*, sonotrode tip) with a diameter of 2 mm. The operational settings of the UW process for polymer-to-polymer welding are listed in Table 1. The laser-cut electrodes were spot welded on the polymer substrate from the rear side of the electrodes (*i.e.*, polymer-to-polymer contact) at a frequency of 30 kHz for 1 s for each spot. The spot welding was evenly applied on the polymer substrates (see the Purdue Logo in Fig. 1) to prevent potential delamination and stress contributors for crack initiation and propagation under harsh deformation conditions, such as repetitive bending and twisting.

2.3. Characterization methods

Scanning electron microscopy (SEM, Hitachi S-4800) and optical microscopy (AMScope) were used to analyze the microstructure of the printings. The surface roughness of the as-cold sprayed samples was measured by a surface roughness tester (AMTAST). A uniaxial tensile test machine (Mark-10) was used to characterize the tensile strength of the resultant printing and the shear adhesion strength of the ultrasonic spot welds. A digital multimeter (Agilent/HP 34401A) was used to measure the electrical resistance of the specimens. A four-point probe system (Jandel, RM3-AR) was employed to measure the sheet resistance of the samples with a constant current of 100 mA at room temperature. The Scotch (3 M magic tape) tape test was conducted to investigate the adhesion strength of the printings. Bending tests were also performed for various bending radii to characterize the flexibility of the specimens. Lastly, an infrared (IR) camera (FLIR A300, FLIR System) was used to characterize the performance of the fabricated microheater. For quantitative characterizations (*i.e.*, 4-point probe, bending, tensile tests), three specimens for each test unit were considered to average the results with standard deviations. All the characterizations were conducted at room temperature.

3. Results and discussion

In this section, first, the microstructure of the CS metallized polymers and resulting printings are studied. Next, characterizations of the mechanical strength of metallized polymers and the UW process are conducted. The electrical conductivity and adhesion strength of the resultant printings are then evaluated. Lastly, a flexible microheater is fabricated to demonstrate the viability of the proposed manufacturing route in FE.

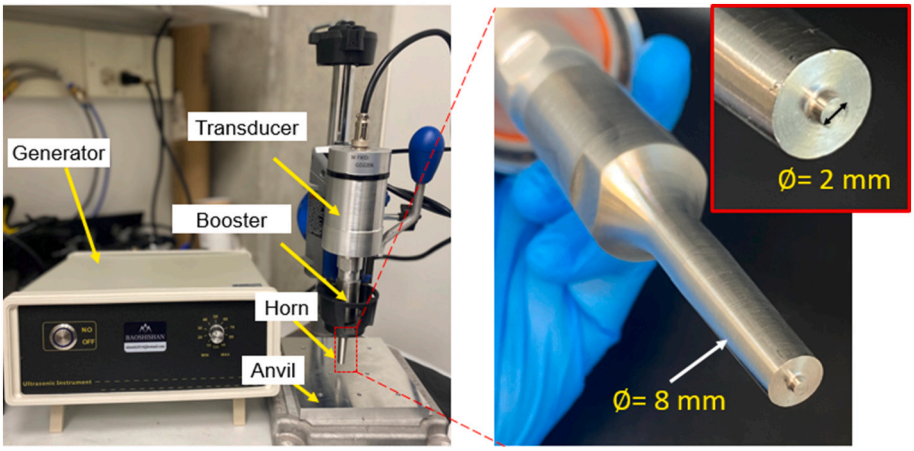

Fig. 3. Representative image of the ultrasonic plastic welding (UW) setup (left panel) with the welding horn and knurl pattern (right panel).

3.1. Characterization of microstructure

Fig. 4a shows the morphology of the feedstock Sn particles used in the CS deposition experiments. The Sn particles are in a size range of 5–45 μm, having a quasi-spherical morphology. Fig. 4b presents the morphology of the as-cold sprayed PET surface. As seen in Fig. 4b, a dense self-bonded micro-rough ($R_a \approx 5.26$ μm) Sn layer on the polymer surface was achieved by CS at operational conditions given in Table 1. No significant crack, erosion, or porosity was observed on the as-cold sprayed layer, which indicates an effective CS particle deposition. The cross-sectional SEM image in Fig. 4b also shows a uniform coating layer on the PET surface with an average thickness of ≈35 μm. Here, it is noteworthy that the as-cold sprayed PET samples can be inherently used as millimeter-scale flexible electronics. As such, CS enables rapid and high-throughput deposition of millimeter-scale (*i.e.*, ≈5 mm linewidth) electrodes on the flexible substrate (PET), thereby having the potential for macro-electronics applications.

Fig. 4c–d show the arbitrarily designed electrodes obtained by the laser-cutting and UW processes, respectively. The femtosecond laser machining enabled scaling-down of the as-cold sprayed Sn electrodes by achieving precise electrode dimensions with ultra-fine features. As seen from the OM images in Fig. 4c, no delamination was observed on the electrodes' surface after the laser-cutting process. Moreover, as shown in Fig. 4d, the resulting electrodes retained high flexibility after the UW process. The resultant printings remained highly conductive under bending deformation without a sign of delamination (see Fig. 4d bottom

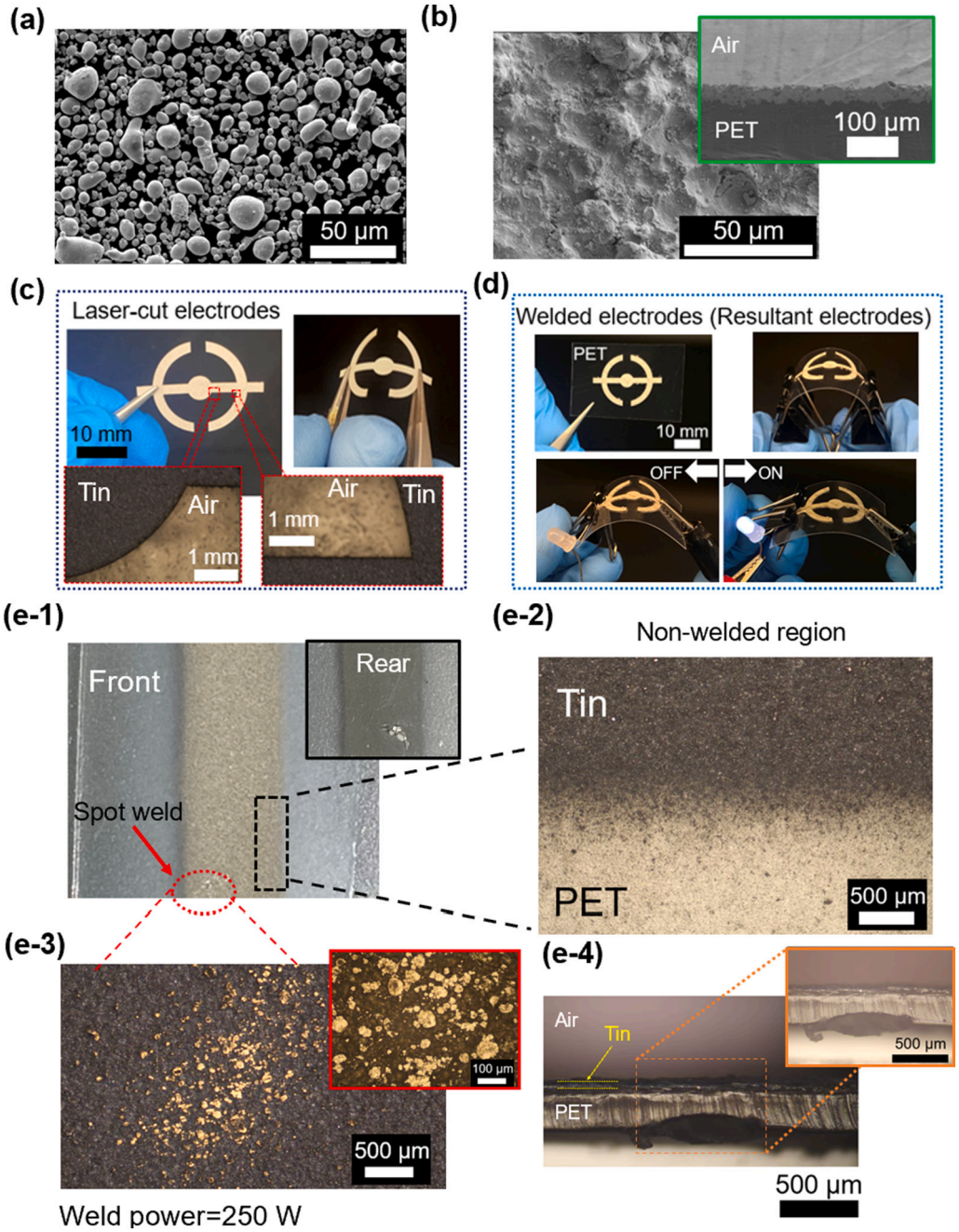

Fig. 4. (a) Morphology of the Sn particles; (b) microstructure of the as-cold sprayed PET surface; (c) laser-cut electrodes from metallized samples; (d) resultant printings after UW process; Image of (e-1) the welded as-cold sprayed sample on bare PET; (e-2) non-welded region; (e-3); welded region; and (e-4) cross-section OM image of the welded zone.

panel).

Fig. 4e presents the further microstructure characterization of the resultant printings. As seen in Fig. 4e-1, some flecks/marks were locally formed on the coating surface where the UW is applied. It is likely attributed to ultrasonic vibration during the welding process. In detail, the rear side of the base polymer (*i.e.*, where the welding horn is contacted) was locally melted due to the mechanical vibrations, resulting in a heat intrusion into the coated layer. Hence, the morphology of the electrodes locally changed where the UW is applied (see Fig. 4-e1). Fig. 4e-2 and e-3 show the surface OM images of the non-welded and welded regions on the printing, respectively. As seen in Fig. 4e-3, the deposited particles agglomerated by forming larger particles near the welding spot. To elaborate this phenomenon, the cross-section morphology of the welded section was investigated. As given in Fig. 4e-4, the contact region of the polymer surfaces was partially melted during the UW process due to the heat accumulation on the polymers. It is noteworthy that the melting pool does not reach the metallized surface, therefore resulting in no significant damage to the as-cold spayed Sn layer. The cross-section image taken near the welding region (Fig. 4e-4) indicates a uniform metal coating on the PET surface, which also proves the non-disruptive effect of the UW process on the as-deposited metal layer. As such, no significant non-uniformity issues between the welding and non-welding zones were observed. Besides, all the samples retained the intrinsic coating properties after UW welding without a noticeable difference in electrical conductivity. The effect of the UW process on the resulting printings is further discussed in Section 3.2.

3.2. *Characteristics of the mechanical strength*

The tensile strength of both bare and as-cold sprayed (metallized)

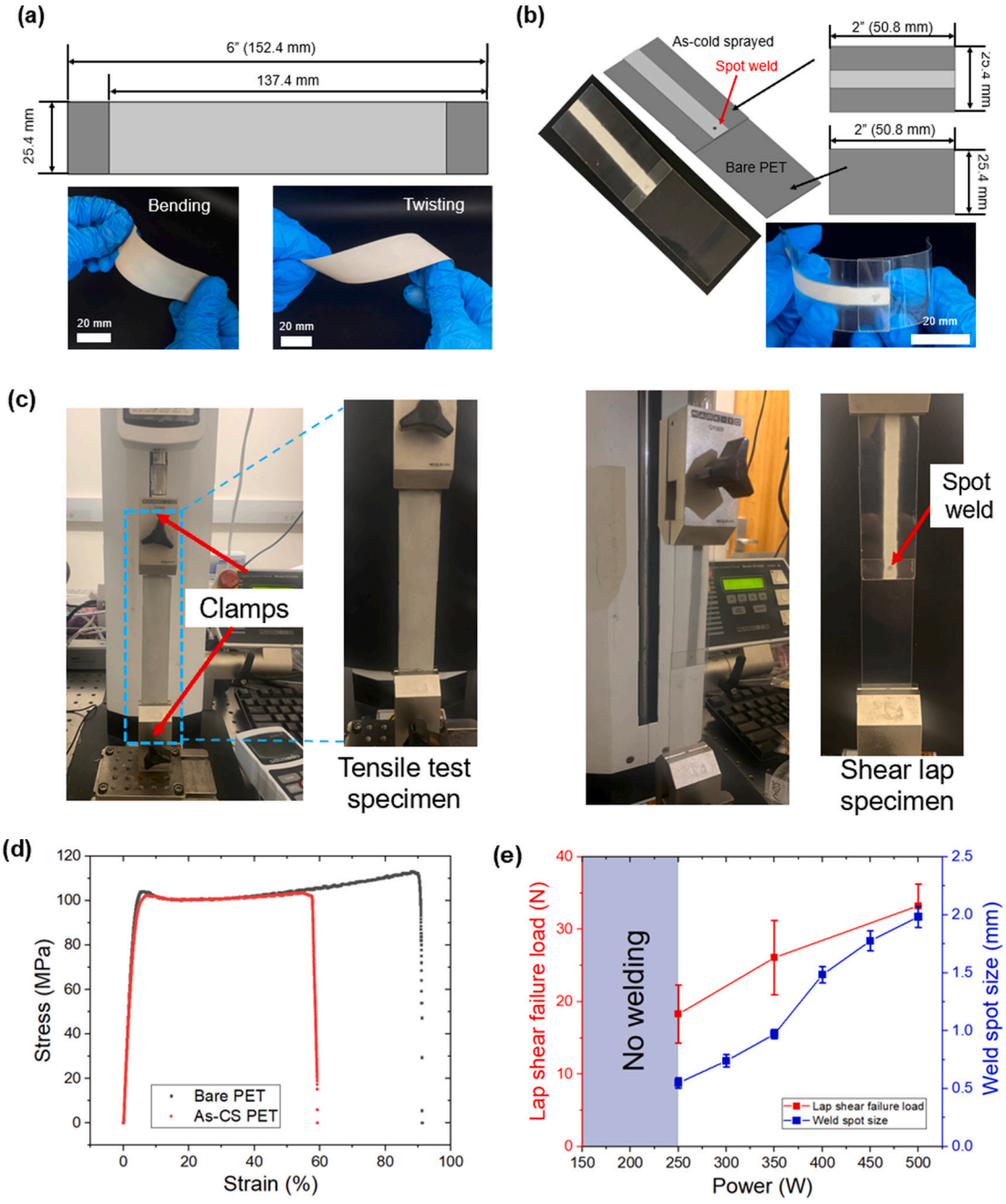

Fig. 5. (a) Tensile test specimens; (b) shear-lap test specimens; (c) tensile test setups; (d) tensile test results for bare and as-cold sprayed PET samples; (e) lap shear strength and weld spot size variation at various ultrasonic welding powers.

PET samples was determined by the uniaxial tensile test according to the ASTM D882 standard (*i.e.*, standard test method for tensile properties of thin plastic sheeting) [40]. The joint (weld) lap shear strength at different welding powers was also characterized based on the ASTM D3163-01 standard [41]. A uniaxial tensile test machine (Mark-10) was used at a displacement rate of 50 mm/min, and each experiment was repeated three times. The representative images of the tensile set specimens and the test setups are presented in Fig. 5a–c. As shown in Fig. 5a, the fabricated flexible electrodes are very durable under bending and twisting deformation. No cracks and delamination were observed on the CS coatings under these deformation conditions. Considering the FE fabricated by the traditional printing approaches (*e.g.*, screen printing, ink-jet printing, *etc.*) are very susceptible to twisting (kinking) deformation, our manufacturing method can address this important limitation of the traditional approaches owing to its strong adhesion-strength, fatigue resistance, and high durability under harsh deformation conditions.

Fig. 5d shows the engineering stress-strain curve of the bare and as-cold sprayed PET samples. As a noteworthy result, the bare PET showed better elongation (≈90 % strain) as compared to the as-cold sprayed PET (≈60 % strain). It is likely attributed to the dense and consolidated metal (Sn) layer on the PET surface (see Fig. 4b), which resulted in a decrease (≈33 %) in the flexibility of the PET polymer after the CS process. The ultimate tensile strength (UTS), however, did not significantly alter for both bare and as-CS polymers. As seen in Fig. 6, bare PET samples have relatively larger (*i.e.*, >5 %) UTS than that of the as-cold sprayed samples. The reasons can be attributed to such local erosions on the as-metallized samples due to the high-speed impingement of the particles onto/into the polymer surface during the CS process [33,42]. However, the erosion on the as-CS PET surface is negligible for FE applications when the overall UTS results are considered. As such, although the CS relatively reduced the flexibility of the PET polymer, the mechanical strength was maintained without significantly compromising the intrinsic polymer properties.

As for the ultrasonically welded electrodes, the effect of the welding input power on the weld spot size and the lap shear failure load was also investigated. Fig. 5e presents the influence of the welding power (*i.e.*, electrical power applied) on weld spot size and lap shear strength at various input powers. Each welding was applied for 1 s at ambient conditions under the same loading conditions. No welding was observed at a power of <250 W, which is likely attributed to insufficient mechanical vibration to join the polymer (PET) surfaces to each other. Successful welding was achieved at the power of ≥250 W to weld the laser-cut electrodes on the substrate surface. However, an excessive rise in the power (*i.e.*, 500 W) resulted in disruptive welding due to high-energy transfer into the substrates (see Fig. S3a, Supporting Information). Moreover, a longer weld time (*i.e.*, 2 s) increased the tendency of void formation on the electrode due to excessive mechanical energy intrusion into the substrates and the Sn coating (Fig. S3b, Supporting Information).

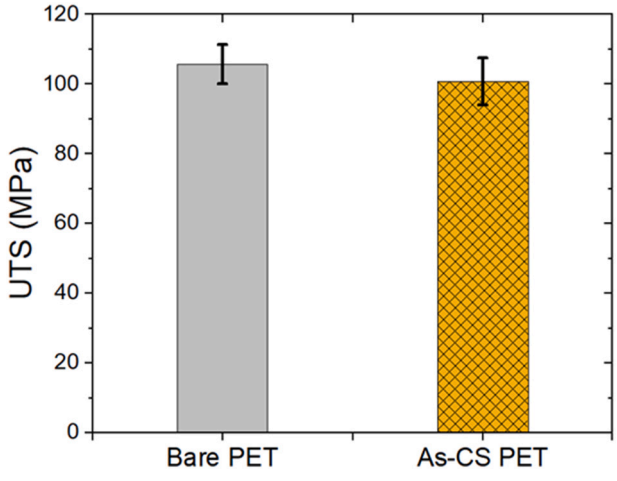

Fig. 6. Ultimate tensile strength of the bare and as-cold sprayed PET samples.

In Fig. 5e, we also characterized the effect of the input power on weld spot size, which was measured from the rear side of the substrate. As seen in Fig. 5e, the spot size increased with higher welding powers. The minimum average spot size was obtained at around 500–550 μm at an input power of 250 W. Here, it is noteworthy that the spot size strictly depends on the dimensions of the welding tip (see Fig. 3, right panel). In the present work, using a horn (8 mm diameter) including a 2-mm diameter welding tip resulted in an equivalent weld spot size of 500–550 μm at the welding power of 250 W. It is important to note that smaller spot sizes could be further achieved by using a narrower welding tip (<2 mm), which can further lead to the welding of higher-resolution (<500 μm linewidth) electrodes on the base polymer substrate. Under these configurations, the proposed manufacturing route in this study is comparable with the traditional printing methods in terms of printing line resolution. Moreover, owing to the flexibility of the femtosecond laser cutting process, the proposed approach can enable high-precision geometric engineering fabrication of FE such as fractal design circuits, thereby having promising potential for flexible design and ultra-fine patterning over the traditional printing techniques.

Lastly, the joint lap shear load at different welding powers was evaluated according to the ASTM D3163-01 standard [41]. As seen in Fig. 5e, the lap shear failure load increased at higher weld powers. It is attributed to more heat intrusion into the polymer surface at higher powers, which facilitated the better cohesion of the materials, resulting in a larger shear failure load. Although higher weld powers increased the shear strength of the welding, it has a disruptive effect on the printing quality (see Fig. S3a, Supporting Information). Taken together, considering small spot size and low-energy consumption, the welding power of 250 W was selected for the following characterization studies on electrical performance and device fabrication.

3.3. Characterization of electrical performance

The electrical resistivity of the as-sprayed and resulting electrodes was calculated using Eq. (1) [43], where 4.532 is the correction factor, R_s is the average sheet resistance (Ω/sq), ρ is the resistivity (Ωm), and t is the sheet thickness (m). R_s value was obtained as 6.81 mΩ/sq from the 4-point probe device measurements while the film thickness was measured as ≈35 μm from the cross-section SEM image in Fig. 4b. As such, the resistivity was calculated as 1.08×10^{-6} Ω·m, which is only one order less than the bulk resistivity of Sn (*i.e.*, 1.1×10^{-7} Ω·m), thereby indicating an excellent electrical conductivity to functionalize the resulting printings in numerous FE applications.

$$\rho = 4.532 \times R_s \times t \tag{1}$$

As shown in Fig. 7a, we also tested the electrical performance of the resultant printings for the test units (*i.e.*, a conduction path in a size of 5 mm × 50 mm) under 1000 bending cycles with various bending radii. For the printed samples, evenly distributed 10 ultrasonic spot welding were applied using the UW process settings given in Table 1. No noticeable change in the electrical resistance was observed in the electrodes right after the UW under no deformation.

The resultant printings, however, showed higher resistance (*i.e.*, lower conductivity) as compared to the as-cold sprayed samples under bending cycles as given in Fig. 7a. The reason lies in the UW process, which increased the stress concentration locally in the polymer substrate. This phenomenon can be better seen from the optical microscopy analysis in Fig. 4e-4, in which some stress contributors (*e.g.*, sharp edges) are formed near the welding regions that could propagate with bending loading, thereby resulting in higher electrical resistance. Although the resultant printings have lower conductivity than the as-cold sprayed samples, the relative resistance (R/R_0) change stayed <200 % for the

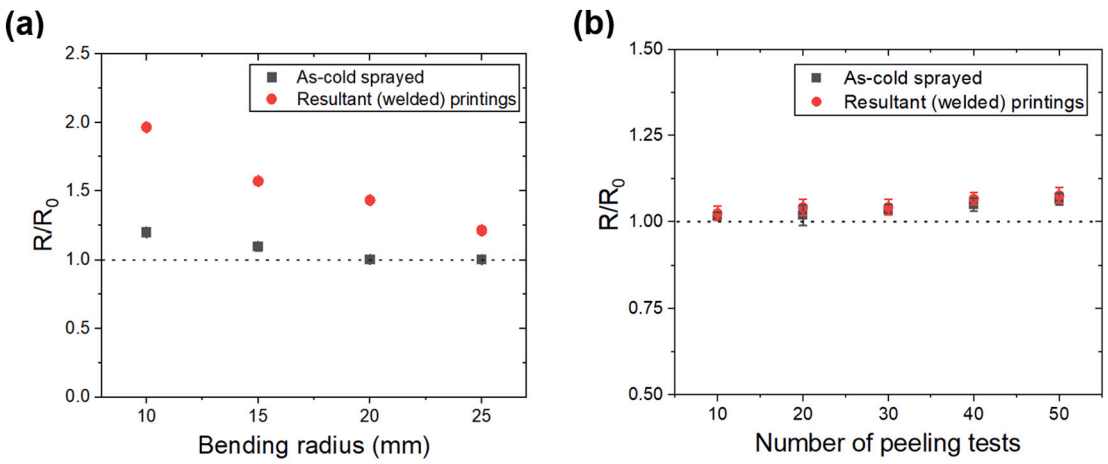

Fig. 7. (a) Relative resistance (R/R_0) change of electrodes under different bending radii; (d) the R/R_0 variation of the as-sprayed and resultant printings under various Scotch tape peeling cycles.

resultant printings. At the higher bending radius (*i.e.*, 20, 25 mm), the R/R_0 difference between the as-sprayed and the resultant printings is observed as <50 %. After the bending tests, no obvious damage in the printings was detected by visual assessment, which confirms the strong adhesion between the cold spray coating and the substrate.

We further investigated the adhesion performance of the printings for the test units (*i.e.*, conduction path in a size of 5 mm × 30 mm) considering the relative resistance (R/R_0) change. Fig. 7b presents the variation of the R/R_0 under peeling test cycles using Scotch tape (3 M Magic). No substantial alteration in the R/R_0 of the electrodes was observed. All the electrodes maintained high-electrical conductivity under the peeling tests. The Scotch tape test confirmed the strong adhesion between the as-cold sprayed Sn layer and the PET polymer substrate before and after the UW process, which also proved the seamless contact of the electrodes to the polymer (PET) substrate.

3.4. Applications and prospect

To show the feasibility and applicability of the proposed approach in printed electronics, a serpentine-shaped flexible resistive microheater was fabricated through the described manufacturing route. The microheater was intentionally selected as a demonstration owing to its wide applications in gas sensing, micro-electro-mechanical (MEMS) devices, biological applications (*e.g.*, cell culture, DNA amplification), and most recently in rapid detection/diagnosis of COVID-19 pandemic [44,45]. As shown in Fig. 8a, the microheater having a linewidth of 500 μm with ultra-fine features was precisely fabricated. Moreover, based on the optical microscope analysis in Fig. 8a (bottom panel), no noticeable delamination in electrodes was observed after the UW process.

The performance of the microheater was tested under various input voltages (*i.e.*, 2.5, 5, 7.5 V) supplied by a DC power generator (Korad, KD6003D). Figs. 8b shows the temperature distribution averaged from a specific area of the heater (see Fig. 8d, left panel). In the analysis, the voltages were supplied to the heater for 2 min followed by the cool-down to room temperature. As seen in Fig. 8b, the average temperature reached the highest value after 80 s, and took approximately 60 s to cool down to room temperature after turn-off the power. The local maximum temperatures in the area of interest at the applied voltages were also plotted in Fig. 8c. The microheater showed a quasi-linear trend in maximum temperature with increasing voltage values. The maximum temperature reached up to 135 °C at such a low input voltage of 2 V owing to the dense-serpentine structure of the microheater in a small area (*i.e.*, 10 × 10 mm^2).

The IR camera images in Fig. 8d represent the flexible microheater under deformation, which also demonstrate the performance and stability of the heater under bending conditions. The microheater maintained its functionality under bending deformation without compromising structural integrity and reliability. The results suggest that the fabricated microheater can be successfully used in numerous applications where stable and accurate thermal stimuli are required such as wearable devices, biomedical, microfluidic, defrosting, and defogging applications. The results also prove that the described manufacturing platform can be effectively employed in the rapid and precise fabrication of microelectronics such as a microheater without the need for high-temperature post-sintering and dedicated vacuum/mask equipment.

Besides, the proposed manufacturing route can be also applied to different substrate materials such as polyimide (PI) (*i.e.*, also known as Kapton film), which is one of the highly demanded materials for wearable electronics, sensing, and smart film applications owing to its high thermal resistance, stability, flexibility, and excellent dielectric and mechanical properties [46–48]. For that, through the described manufacturing platform, we welded the laser-cut arbitrarily designed Sn electrode (*i.e.*, Purdue logo) on the PI substrate. As seen in Fig. 9, the proposed approach was successfully applied to a PI surface, proving its versatility in FE. The resultant printing maintained its flexibility and conductivity without significantly compromising intrinsic polymer and Sn coating properties. Considering cold spraying of metal particles on thermosets such as PI is currently a major challenge in the CS literature [49,50], the established manufacturing platform in this study can also address this crucial issue in CS research. More specifically, the custom-designed electrodes (*i.e.*, cold sprayed + laser cut) can be easily transferred on thermoset polymers *via* the ultrasonic plastic welding process in a manner that the intrinsic advantages of the CS technique (*i.e.*, low-cost, high electrical conductivity, strong adhesion strength, corrosion resistance, *etc.*) can be exploited in a wide range of printed FE applications. As such, the results indicate that the proposed manufacturing platform has tremendous potential for rapid and scalable production of FE on various polymer substrates with custom tailoring.

4. Conclusion

In this study, we introduced a novel manufacturing route that enables rapid production of high-resolution and custom-designed flexible electronics without significantly compromising intrinsic polymer and functional coating properties. The proposed platform sequentially involves cold spray metallization, femtosecond laser machining, and ultrasonic plastic welding processes. First, millimeter-scale electrically conductive Tin (Sn) traces were directly written on the PET surface by cold spraying. The subsequent laser cutting led to high-resolution (500

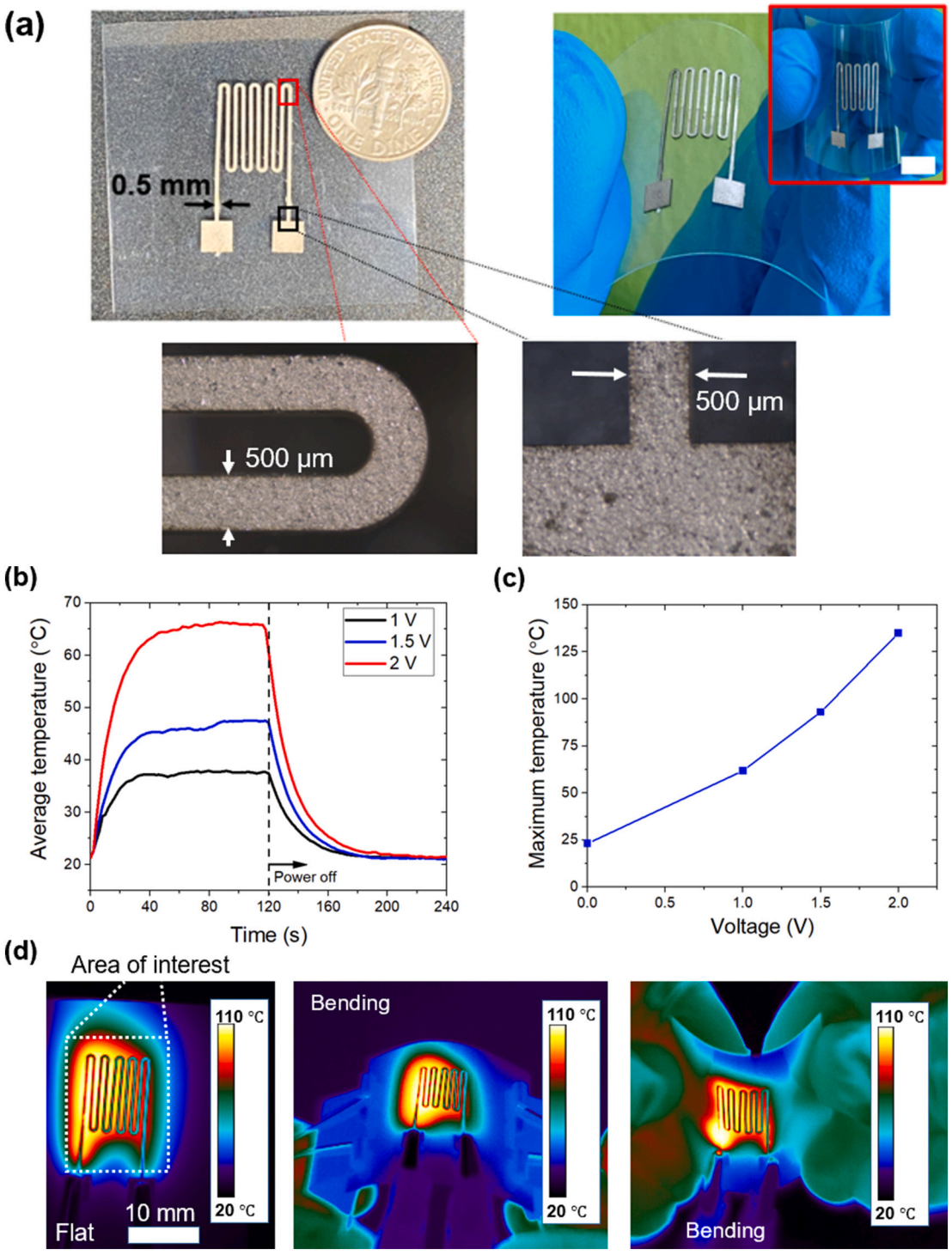

Fig. 8. (a) Digital (upper panel) and OM (bottom panel) images of the fabricated flexible microheater; (b) temperature profile of the microheater at different voltage inputs; (c) The maximum temperature variation of the microheater under different voltages; (d) demonstration of the microheater under different loading conditions.

µm linewidth) electrodes. Lastly, through the ultrasonic welding (UW) process, the laser-cut electrodes were welded on a base polymer to enhance the mechanical resilience of the electrodes by constituting resilient and conformal FE. The conclusions are given as follows:

- Unlike the traditional printing approaches, the proposed manufacturing route requires no masking, vacuum equipment, and high-temperature sintering, thereby having the potential for effective and efficient printing on low-thermal budget substrates such as PET.
- The resulting high-resolution printings showed excellent electrical conductivity (0.91×10^6 S·m^{-1}), flexibility (60 % elongation under the tensile test), and adhesion strength (*i.e.*, <5 % change in the R/R_0 after 50 peeling cycles) without significantly compromising intrinsic polymer and functional coating properties.

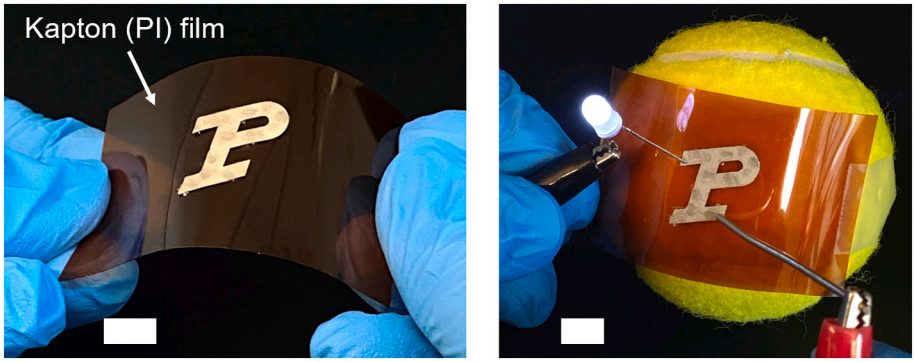

Fig. 9. Fabrication of the arbitrarily designed Sn electrode on a flexible polyimide (PI) film through the proposed manufacturing route (Scale bar = 10 mm).

- The fabricated flexible microheater (10 × 10 mm^2) demonstrated the viability and applicability of the proposed method in flexible microelectronics.
- The proposed manufacturing route was also successfully applied to a thermosetting polymer (Kapton film), which also proved the versatility of the manufacturing route for thermosetting plastics.
- Comprising low-cost coating materials (*e.g.*, Sn powders = 39$/lb) without a need for high-temperature post-annealing, the established manufacturing platform can potentially open up a promising route toward rapid, scalable, and low-cost production of flexible microelectronics.

CRediT authorship contribution statement

Semih Akin: Conceptualization, methodology, formal analysis, investigation, design, experiments, characterization, data curation, application, writing manuscript, review & editing;

Seunghwan Jo: Experiments, characterization, review & editing;

Martin B.G. Jun: Conceptualization, methodology, resources, supervision, review & editing.

All authors commented on the manuscript.

Declaration of competing interest

The authors declare that they have no known competing financial interests or personal relationships that could have appeared to influence the work reported in this paper.

Appendix A. Supplementary data

Supplementary data to this article can be found online at https://doi.org/10.1016/j.jmapro.2022.12.035.

References

[1] Zhang Z, Wang Y, Wang Q, Shang L. Smart film actuators for biomedical applications. Small 2022. https://doi.org/10.1002/smll.202105116.
[2] Cho S, Chang T, Yu T, Lee CH. Smart electronic textiles for wearable sensing and display. Biosens 2022;12:222. https://doi.org/10.3390/BIOS12040222. 2022;12:222.
[3] Tian B, Fang Y, Liang J, Zheng K, Guo P, Zhang X, et al. Fully printed stretchable and multifunctional E-textiles for aesthetic wearable electronic systems. Small 2022:18. https://doi.org/10.1002/smll.202107298.
[4] Chang T, Akin S, Kim MK, Murray L, Kim B, Cho S, et al. Programmable dual regime spray for large-scale and custom-designed electronic textiles. Adv Mater 2021:2108021. https://doi.org/10.1002/adma.202108021.
[5] Heng W, Solomon S, Gao W. Flexible electronics and devices as human-machine interfaces for medical robotics. Adv Mater 2022:2107902. https://doi.org/10.1002/adma.202107902.
[6] Shi Q, He T, Lee C. More than energy harvesting – combining triboelectric nanogenerator and flexible electronics technology for enabling novel micro-/nano-systems. Nano Energy 2019;57:851–71. https://doi.org/10.1016/j.nanoen.2019.01.002.
[7] Liao Y, Zhang R, Qian J. Printed electronics based on inorganic conductive nanomaterials and their applications in intelligent food packaging. RSC Adv 2019;9:29154–72. https://doi.org/10.1039/c9ra05954g.
[8] Sekine C, Tsubata Y, Yamada T, Kitano M, Doi S. Recent progress of high performance polymer OLED and OPV materials for organic printed electronics. Sci Technol Adv Mater 2014:15. https://doi.org/10.1088/1468-6996/15/3/034203.
[9] Wiklund J, Karakoç A, Palko T, Yigitler H, Ruttik K, Jäntti R, et al. A review on printed electronics: fabrication methods, inks, substrates, applications and environmental impacts. J Manuf Mater Process 2021;5:89. https://doi.org/10.3390/jmmp5030089.
[10] Bonnassieux Y, Brabec CJ, Cao Y, Carmichael TB, Chabinyc ML, Cheng KT, et al. The 2021 flexible and printed electronics roadmap. Flex Print Electron 2021;6:023001. https://doi.org/10.1088/2058-8585/abf986.
[11] Huang Q, Zhu Y. Printing conductive nanomaterials for flexible and stretchable electronics: a review of materials, processes, and applications. Adv Mater Technol 2019;4:1–41. https://doi.org/10.1002/admt.201800546.
[12] Nayak L, Mohanty S, Kumar Nayak S, Ramadoss A. A review on inkjet printing of nanoparticle inks for flexible electronics. J Mater Chem C 2019;7:8771. https://doi.org/10.1039/c9tc01630a.
[13] Hamad A, Mian A, Khondaker SI. Direct-write inkjet printing of nanosilver ink (UTDAg) on PEEK substrate. J Manuf Process 2020;55:326–34. https://doi.org/10.1016/j.jmapro.2020.04.046.
[14] He P, Cao J, Ding H, Liu C, Neilson J, Li Z, et al. Screen-printing of a highly conductive graphene ink for flexible printed electronics. ACS Appl Mater Interfaces 2019;11:32225–34. https://doi.org/10.1021/acsami.9b04589.
[15] Secor EB, Lim S, Zhang H, Frisbie CD, Francis LF, Hersam MC. Gravure printing of graphene for large-area flexible electronics. Adv Mater 2014;26:4533–8. https://doi.org/10.1002/ADMA.201401052.
[16] Zhu J, Han D, Wu X, Ting J, Du S, Arias AC. Highly flexible transparent micromesh electrodes via blade-coated polymer networks for organic light-emitting diodes. ACS Appl Mater Interfaces 2020;12:31687–95. https://doi.org/10.1021/ACSAMI.0C07299/SUPPL_FILE/AM0C07299_SI_001.PDF.
[17] Chen YD, Nagarajan V, Rosen DW, Yu W, Huang SY. Aerosol jet printing on paper substrate with conductive silver nano material. J Manuf Process 2020;58:55–66. https://doi.org/10.1016/j.jmapro.2020.07.064.
[18] Wilkinson NJ, Smith MAA, Kay RW, Harris RA. A review of aerosol jet printing—a non-traditional hybrid process for micro-manufacturing. Int J Adv Manuf Technol 2019;105:4599–619. https://doi.org/10.1007/s00170-019-03438-2.
[19] Valentine AD, Busbee TA, Boley JW, Raney JR, Chortos A, Kotikian A, et al. Hybrid 3D printing of soft electronics. Adv Mater 2017;29:1703817. https://doi.org/10.1002/adma.201703817.
[20] Suganuma K. Introduction to printed electronicsvol. 74. New York, NY: Springer New York; 2014. https://doi.org/10.1007/978-1-4614-9625-0.
[21] Zhang H, Moon SK, Ngo TH. 3D printed electronics of non-contact ink writing techniques: status and promise. Int J Precis Eng Manuf - Green Technol 2020;7:511–24. https://doi.org/10.1007/s40684-019-00139-9.
[22] Maddipatla D, Narakathu BB, Atashbar M. Recent Progress in manufacturing techniques of printed and flexible sensors: a review. Biosensors 2020;10:199. https://doi.org/10.3390/bios10120199.
[23] Goh GL, Zhang H, Chong TH, Yeong WY. 3D printing of multilayered and multimaterial electronics: a review. Adv Electron Mater 2021;7:2100445. https://doi.org/10.1002/aelm.202100445.
[24] Khan Y, Thielens A, Muin S, Ting J, Baumbauer C, Arias AC. A new frontier of printed electronics: flexible hybrid electronics. Adv Mater 2020;32:1905279. https://doi.org/10.1002/adma.201905279.
[25] Akin S, Lee S, Jo S, Ruzgar DG, Subramaniam K, Tsai J-T, et al. Cold spray-based rapid and scalable production of printed flexible electronics. Addit Manuf 2022;60:103244. https://doi.org/10.1016/J.ADDMA.2022.103244.
[26] Yin S, Cavaliere P, Aldwell B, Jenkins R, Liao H, Li W, et al. Cold spray additive manufacturing and repair: fundamentals and applications. Addit Manuf 2018;21:628–50. https://doi.org/10.1016/j.addma.2018.04.017.
[27] Raoelison RN, Xie Y, Sapanathan T, Planche MP, Kromer R, Costil S, et al. Cold gas dynamic spray technology: a comprehensive review of processing conditions for various technological developments till to date. Addit Manuf 2018;19:134–59. https://doi.org/10.1016/j.addma.2017.07.001.

[28] Che H, Chu X, Vo P, Yue S. Metallization of various polymers by cold spray. J Therm Spray Technol 2018;27:169–78. https://doi.org/10.1007/s11666-017-0663-1.
[29] Che H, Liberati AC, Chu X, Chen M, Nobari A, Vo P, et al. Metallization of polymers by cold spraying with low melting point powders. Surf Coat Technol 2021;418:127229. https://doi.org/10.1016/J.SURFCOAT.2021.127229.
[30] Che H, Vo P, Yue S. Metallization of carbon fibre reinforced polymers by cold spray. Surf Coat Technol 2017;313:236–47. https://doi.org/10.1016/j.surfcoat.2017.01.083.
[31] Kim YW, Akin S, Yun H, Xu S, Wu W, Byung M, et al. Enhanced performance of triboelectric nanogenerators and sensors via cold spray particle deposition. ACS Appl Mater Interfaces 2022. https://doi.org/10.1021/ACSAMI.2C09367.
[32] An S, Joshi B, Yarin AL, Swihart MT, Yoon SS. Supersonic cold spraying for energy and environmental applications: one-step scalable coating technology for advanced micro- and nanotextured materials. Adv Mater 2020;32:1905028. https://doi.org/10.1002/adma.201905028.
[33] Akin S, Tsai J-T, Park MS, Jeong YH, Jun M. Fabrication of electrically conductive patterns on ABS polymer using low-pressure cold spray and electroless plating. J Micro Nano-Manuf 2021:8. https://doi.org/10.1115/1.4049578.
[34] Akin S, Wu P, Tsai J-T, Nath C, Chen J, Jun MB-G. A study on droplets dispersion and deposition characteristics under supersonic spray flow for nanomaterial coating applications. Surf Coat Technol 2021;426:127788. https://doi.org/10.1016/j.surfcoat.2021.127788.
[35] Li W, Yang K, Yin S, Yang X, Xu Y, Lupoi R. Solid-state additive manufacturing and repairing by cold spraying: a review. J Mater Sci Technol 2018;34:440–57. https://doi.org/10.1016/j.jmst.2017.09.015.
[36] Jo S, Akin S, Park MS, Jun MBG. Selective metallization on glass surface by laser direct writing combined with supersonic particle deposition. Manuf Lett 2022;31:64–8. https://doi.org/10.1016/j.mfglet.2021.07.009.
[37] Akin S, Gabor T, Jo S, Joe H, Tsai JT, Park Y, et al. Dual regime spray deposition based laser direct writing of metal patterns on polymer substrates. J Micro Nano-Manuf 2020:8. https://doi.org/10.1115/1.4046282.
[38] Bhudolia SK, Gohel G, Leong KF, Islam A. Advances in ultrasonicwelding of thermoplastic composites: a review. Materials (Basel) 2020;13:1284. https://doi.org/10.3390/ma13061284.
[39] Wang Y, Rao Z, Liao S, Wang F. Ultrasonic welding of fiber reinforced thermoplastic composites: current understanding and challenges. Compos Part A Appl Sci Manuf 2021;149:106578. https://doi.org/10.1016/j.compositesa.2021.106578.
[40] ASTM D 882-02. Standard Test Method for Tensile Properties of Thin Plastic Sheeting. ASTM International; 2002.
[41] Astm D 3163-01. In: Standard Test Method for Determining Strength of Adhesively Bonded Rigid Plastic Lap-Shear Joints in Shear by Tension Loading. Standards. 01; 2001. p. 1–3.
[42] Tsai JT, Akin S, Zhou F, Bahr DF, Jun MBG. Establishing a cold spray particle deposition window on polymer substrate. J. Therm. Spray. Technol. 2021;30:1069–80. https://doi.org/10.1007/s11666-021-01179-x.
[43] Smits FM. Measurement of sheet resistivities with the four-point probe. Bell Syst Tech J 1958;37:711–8. https://doi.org/10.1002/j.1538-7305.1958.tb03883.x.
[44] Jeroish ZE, Bhuvaneshwari KS, Samsuri F, Narayanamurthy V. Microheater: material, design, fabrication, temperature control, and applications—a role in COVID-19. Biomed Microdevices 2022;24:3. https://doi.org/10.1007/s10544-021-00595-8.
[45] Yang Y, Li S, Xu H, Xu Y, Chen Y. Fabrication of flexible microheater with tunable heating capabilities by direct laser writing and selective electrodeposition. J Manuf Process 2022;74:88–99. https://doi.org/10.1016/j.jmapro.2021.11.045.
[46] Lin LK, Tsai JT, DÄ-Az-Amaya S, Oduncu MR, Zhang Y, Huang PY. Antidelaminating, thermally stable, and cost-effective flexible kapton platforms for nitrate sensors, mercury aptasensors, protein sensors, and p-type organic thin-film transistors. ACS Appl. Mater. Interfaces 2021;13:11369–84. https://doi.org/10.1021/acsami.0c18426.
[47] Rau DA, Herzberger J, Long TE, Williams CB. Ultraviolet-assisted direct ink write to additively manufacture all-aromatic polyimides. ACS Appl Mater Interfaces 2018;10:34828–33. https://doi.org/10.1021/ACSAMI.8B14584/ASSET/IMAGES/LARGE/AM-2018-145849_0003.JPEG.
[48] Hegde M, Meenakshisundaram V, Chartrain N, Sekhar S, Tafti D, Williams CB, et al. 3D printing all-aromatic polyimides using mask-projection stereolithography: processing the nonprocessable. Adv Mater 2017;29:1701240. https://doi.org/10.1002/ADMA.201701240.
[49] Ganesan A, Yamada M, Fukumoto M. Cold spray coating deposition mechanism on the thermoplastic and thermosetting polymer substrates. J Therm Spray Technol 2013;22:1275–82. https://doi.org/10.1007/s11666-013-9984-x.
[50] Della Gatta R, Perna AS, Viscusi A, Pasquino G, Astarita A. Cold spray deposition of metallic coatings on polymers: a review. J Mater Sci 2022;57:27–57. https://doi.org/10.1007/s10853-021-06561-2.